

~~CONFIDENTIAL~~

Copy 221  
RM E51C06

NACA RM E51C06

E 51 C 06

~~53 29 90~~



014637

TECH LIBRARY KAFB, NM

# RESEARCH MEMORANDUM

AERODYNAMIC CHARACTERISTICS OF FOUR BODIES OF REVOLUTION  
SHOWING SOME EFFECTS OF AFTERBODY SHAPE AND FINENESS  
RATIO AT FREE-STREAM MACH NUMBERS FROM 1.50 TO 1.99

By Robert J. Cohen

Lewis Flight Propulsion Laboratory  
Cleveland, Ohio

~~SECRET~~  
This document contains classified information affecting the National Defense of the United States within the meaning of the Espionage Act, USC 50c1 and 51. Its transmission or communication to any person other than a member of an authorized person is prohibited.  
Information on classification is limited only to persons in the military and naval services of the United States, and to civilian officers and employees of the Federal Government who have a legitimate interest in it, and to United States citizens of known loyalty and discretion who of necessity must be informed thereof.

## NATIONAL ADVISORY COMMITTEE FOR AERONAUTICS

WASHINGTON

May 22, 1951

~~CONFIDENTIAL~~

319.98/13

~~53 29 90~~

6664

~~CONFIDENTIAL~~

## NATIONAL ADVISORY COMMITTEE FOR AERONAUTICS

RESEARCH MEMORANDUM

AERODYNAMIC CHARACTERISTICS OF FOUR BODIES OF REVOLUTION SHOWING  
SOME EFFECTS OF AFTERBODY SHAPE AND FINENESS RATIO AT  
FREE-STREAM MACH NUMBERS FROM 1.50 TO 1.99

By Robert J. Cohen

## SUMMARY

As part of a general program to determine the aerodynamic characteristics of bodies of revolution operating at supersonic speeds and at moderate angles of attack, four model configurations of fineness ratios 12.2 and 14.2 were investigated in the NACA Lewis 8- by 6-foot supersonic tunnel. Force, moment, and base-pressure coefficients were measured for a range of angles of attack from  $0^\circ$  to  $10^\circ$  at free-stream Mach numbers of 1.50, 1.60, 1.79, and 1.99 within a range of Reynolds numbers from  $29 \times 10^6$  to  $40 \times 10^6$  based on body length.

At zero angle of attack the experimental results of the investigation indicated that the increase in model fineness ratio from 12.2 to 14.2, by adding a cylindrical section, did not appreciably affect the total drag, measured base drag, or fore drag coefficient. Boattailing, however, increased the model fore drag but decreased the measured base drag considerably, resulting in a considerable decrease of total drag. Decreasing the boattail convergence from 0.174 to 0.074 increased the measured base drag but decreased the model fore drag with a subsequent further decrease in total drag. At angle of attack the increase of model fineness ratio, by adding a cylindrical section, resulted in an increase in the incremental fore drag and lift coefficients based on maximum cross-sectional area. The center of pressure location as a percent of the model length was unchanged by the increase in fineness ratio. Boattailing produced a decrease in lift and incremental fore drag and a forward movement of the center of pressure location with a resultant increase in pitching moment about the first station of maximum cross section located approximately 7.5 maximum diameters from the nose. Decreasing the boattail convergence did not appreciably affect the lift but increased the incremental fore drag and the pitching moment about the first station of maximum cross section.

**PERMANENT**PROOF~~CONFIDENTIAL~~

Comparison of experimental results with results calculated with the method presented by Allen (reference 1), which approximates the effects of viscosity on an inclined body of revolution, indicated that this method was a significant improvement over the linearized potential theory in predicting the forces on a slender body of revolution, particularly at the higher angles of attack. For the cylindrical afterbody models, the use of Allen's method overestimated the lift coefficient but predicted the center of pressure location quite accurately. The lift coefficient was predicted for the boattail model at the low free-stream Mach number but the center of pressure location was estimated too far ahead of the base by the method presented by Allen.

### INTRODUCTION

A series of bodies of revolution have been investigated in the 8- by 6-foot supersonic tunnel as part of a general program to determine the aerodynamic characteristics of bodies of revolution at supersonic speeds and moderate angles of attack. For this investigation, the parabolic body of revolution of references 2 and 3 was modified aft of the station of maximum diameter (station 45) by changes in the afterbody contours.

The purposes of this investigation were to provide aerodynamic force and moment data for bodies of revolution and to determine the effects on the aerodynamic characteristics produced by changes in the model fineness ratio, afterbody shape, and boattail convergence. The experimental data are compared with values calculated by existing theoretical methods (references 1 and 4) to provide a further evaluation of these methods.

The four configurations were investigated for a range of angles of attack from  $0^\circ$  to  $10^\circ$  and at free-stream Mach numbers of 1.50, 1.60, 1.79, and 1.99. The Reynolds number based on body length was approximately  $35 \times 10^6$ .

### SYMBOLS

The following symbols are used in this report:

- $C_D$  total drag coefficient,  $D/q_0 S_{max}$
- $C_{D,b}$  base pressure drag coefficient,  $-C_{p,b} \frac{S_b}{S_{max}}$
- $C_{d,c}$  drag coefficient of circular cylinder section based on cross-flow Mach number and Reynolds number based on maximum body diameter

$\Delta C_{D,F}$	incremental fore drag coefficient, $(C_{D}-C_{D,b})$ at angle of attack minus $(C_{D}-C_{D,b})$ at zero angle of attack
$C_{D,p}$	boattail surface pressure drag coefficient
$C_L$	lift coefficient, $L/q_0 S_{max}$
$C_{m,45}$	pitching-moment coefficient about station 45, $\frac{m_{45}}{q_0 S_{max} l}$
$C_N$	normal force coefficient, $\frac{N}{q_0 S_{max}}$
$C_{p,b}$	base pressure coefficient, $(p-p_0)/q_0$
D	drag force
$D_b$	base diameter
$D_s$	sting diameter
d	center of pressure location ahead of base measured along body axis, $\frac{C_{m,45}}{C_N} l + (l-45)$
L	lift force
l	model length
M	Mach number
$m_{45}$	pitching moment about station of maximum cross section, approximately 7.5 maximum diameters from nose (station 45)
N	normal force
p	static pressure
q	dynamic pressure, $\frac{\gamma}{2} \rho M^2$
$S_b$	area of base
$S_{max}$	maximum cross-sectional area
$\alpha$	angle of attack
$\gamma$	ratio of specific heats (1.40)
$\eta$	ratio of drag coefficient of circular cylinder of finite length to that for cylinder of infinite length

## Subscripts:

- b     model base  
p     pressure  
s     sting  
O     free-stream conditions

2127

## APPARATUS AND PROCEDURE

Schematic diagrams of the configurations of this investigation are presented in figure 1. The equations and the coordinates of the models are given in table I.

The basic body common to models 1, 2, 3, and 4 consisted of a sharp-nose parabolic contoured body of revolution identical to the portion of the NACA RM-10 fuselage (of references 2 and 3) ahead of the station of maximum cross section approximately 7.5 maximum diameters from the nose (station 45), followed by a cylindrical section approximately 2.71 diameters in length.

Models 1 and 2 were formed by attaching a 12-inch boattail section and a 12-inch cylindrical section, respectively, to the basic body. Models 3 and 4 were obtained by inserting a cylindrical section, 11.75 inches in length, between the basic body and the end sections of models 1 and 2, respectively.

The models were sting supported from the main tunnel strut with the strain-gage balance located inside the models. Only the forces on the bodies were measured and no tare corrections were necessary.

The angle of attack of the model was determined by adding to the indicated strut angle a statically calibrated model inclination due to sting and balance deflection resulting from the measured normal forces and moments. The static pressures at the base of the model were measured by four orifices located around the base of the model as shown in figure 1.

Each configuration was investigated at free-stream Mach numbers 1.50, 1.60, 1.79, and 1.99 for a range of angles of attack from  $0^\circ$  to  $10^\circ$ . The average Reynolds number for each model, based on model length, is shown in table II for each free-stream Mach number.

## METHOD OF COMPUTATION AND REDUCTION OF DATA

The measured normal and axial forces were analytically resolved into lift and drag components. Pitching moment was measured about station 45 and is presented in coefficient form.

The experimental results obtained for the models of fineness ratio 14.2 at Mach numbers 1.50 and 1.60 are subject to the effects of model nose shock reflecting from the tunnel walls into the vicinity of the base. For the models of fineness ratio 12.2 at the free-stream Mach number of 1.50, it was expected that the reflected shock intersected the sting downstream of the model base but the base pressure might still be affected as indicated in reference 5. For all models, however, the effect on the force coefficients other than the base drag coefficient was presumed to be comparatively small.

The data at a free-stream Mach number 1.50 for models of fineness ratio 14.2 and 12.2 and the data at a free-stream Mach number of 1.60 for models of fineness ratio 14.2 were probably affected by weak disturbances in the flow (reference 3). Due to the lack of pressure instrumentation no correction to the data could be evaluated. However, the probable magnitude of the effect of reflected nose shock and the weak tunnel disturbances will be discussed and indicated subsequently.

Based on the data presented in reference 6, for the ratio of sting diameter to maximum body diameter of 0.40 and the ratio of unobstructed sting length to maximum body diameter of approximately 2.71, the effect of the sting on the base pressure drag of models 1 and 3 is believed to be negligible. Any further effect of the sting on the boattail surface pressure drag is also presumably quite small. For models 2 and 4, however, it was inferred from the data of reference 5 that the base-pressure drag may be significantly affected by the presence of the sting, but no correction for this effect was feasible.

The theoretical lift, drag, and pitching moment of the bodies were computed from the linearized potential theory (assuming flow follows entire body) presented in reference 4 and the method of reference 1. Based on the conditions of this investigation, an average value of  $\eta = 0.72$  and an average value of  $C_{d,c} = 1.2$  was used for the method of reference 1.

## RESULTS AND DISCUSSION

The variation of lift coefficient (based on maximum cross-sectional area) with angle of attack at four Mach numbers is presented in figure 2

for the four models. These data indicate that the lift curve slope increased with angle of attack and free-stream Mach number for both the cylindrical afterbody and boattailed models. At small angles of attack, however, the lift coefficient was nearly independent of free-stream Mach number.

The calculated variations of lift coefficient with angle of attack based on linearized potential theory and the method of reference 1 are also included in figure 2. Inasmuch as the calculated values are independent of free-stream Mach number, neither potential theory nor the method of reference 1 predicts the increase in lift with free-stream Mach number. In general, potential theory underestimated the lift for all configurations. At high angles of attack the underestimation was more pronounced for the boattailed models (figs. 2(a) and 2(c)) than for the cylindrical afterbody models (figs. 2(b) and 2(d)). At angles of attack below approximately  $4^\circ$ , the theoretical values are in fair agreement with the experimental results for the cylindrical afterbody models. The inability of linearized potential theory to predict the lift above  $4^\circ$  angle of attack may be attributable in part to the effects of viscosity and in part to the inability of the theory to accurately predict the potential flow pressure distribution due to angle of attack as discussed in reference 7.

The method of reference 1 is in good agreement with the lift coefficient data of the boattail models, particularly at the low free-stream Mach numbers as shown in figures 2(a) and 2(c). For the cylindrical afterbody models, however, the calculated lift coefficients overestimate the experimental data at all free-stream Mach numbers, particularly the data at the low free-stream Mach numbers as shown in figures 2(b) and 2(d).

In general, approximating the viscosity effects by the method of reference 1 results in a significant improvement over potential theory in predicting the lift coefficients, especially for the boattail models, and for the cylindrical afterbody models at the higher angles of attack.

For these models, the cross-flow Reynolds number from which the value of  $C_{d,c}$  (used in method of reference 1) is determined falls within the critical range indicated in reference 1. Consequently, the value of  $C_{d,c}$  would vary abruptly and an erratic variation of  $C_L$  would be expected. Examination of all lift data does not, however, reveal any noticeably erratic trends except for a slight decrease in the rate of increase of the lift curve slope for model 2 between  $2^\circ$  and  $4^\circ$  angle of attack. This small deviation may possibly be attributable to the critical cross-flow Reynolds number but is not substantiated by the data of model 4, which more closely approximates a smoothly increasing

2127

lift curve than model 2. Model 4 would be expected to be more sensitive to cross-flow Reynolds number in the critical range because it has a longer cylindrical length than model 2. It was therefore concluded that for these data there was no significant effect on the lift resulting from the variation of the cross-flow Reynolds number in the critical range. The value of  $C_{d,c} = 1.2$  used in the method of reference 1 provides reasonably good agreement between the calculated and experimental values. In addition, the trend of the lift variation is better approximated by the use of a constant value of  $C_{d,c}$  than a variable  $C_{d,c}$  corresponding to the cross-flow Reynolds number at each angle of attack as shown in figure 2(b).

The variation of pitching-moment coefficient with angle of attack for the four configurations is presented in figure 3 at four Mach numbers. Although the pitching-moment coefficient is essentially independent of free-stream Mach number, a small decrease was noted with increasing free-stream Mach number for the boattail model of fineness ratio 14.2 (fig. 3(c)).

As shown in figure 3, the pitching-moment coefficients calculated by both potential theory and the method of reference 1 show an increasing divergence for the arbitrary center of moments chosen in this investigation (station 45). Better agreement was obtained between the calculated values and the experimental pitching-moment coefficients for the cylindrical afterbody models (figs. 3(b) and 3(d)) than for the boattail models (figs. 3(a) and 3(c)). These results, however, appear fortuitous because the agreement between the calculated values and the experimental pitching-moment coefficients will be influenced by the location of the center of moments. (For example, at  $6^\circ$  angle of attack at a free-stream Mach number of 1.50, the method of reference 1 would overestimate the pitching-moment coefficient for model 2 about station 0 by approximately 40 percent, whereas potential theory would underestimate the experimental results by nearly 30 percent. The same inadequacy of potential theory and the method of reference 1 to predict the pitching-moment characteristics can be demonstrated for the boattail models. It can be concluded that agreement of the calculated with the experimental pitching-moment characteristics was dependent upon the arbitrarily selected center of moments.)

The variation of center of pressure location with angle of attack for the four models is presented in figure 4, as the ratio of its distance from the base to the body length  $d/l$ . The center of pressure moved rearward with increasing angles of attack for the cylindrical afterbody and boattail bodies. The rearward shift of the center of pressure location for the boattail models (figs. 4(a) and 4(c)) was about 30 percent of the model length and for the cylindrical afterbody models (figs. 4(b) and 4(d)) the rearward shift was about 12 percent of the model length.

These results indicate a greater increase in the forces over the boattail section with increasing angle of attack than for the corresponding cylindrical afterbody section.

The center of pressure locations for the cylindrical afterbody models were virtually independent of free-stream Mach number. The maximum rearward shift with increasing free-stream Mach number was about 4 percent of the model length. The boattail models, however, experienced a rearward movement of the center of pressure location of approximately 18 percent of the body length at the low angles of attack to 10 percent at the higher angles of attack as the free-stream Mach number was increased from 1.50 to 1.99.

Comparison of the experimental center of pressure location with the values calculated by the potential theory indicates that the theory predicted the center of pressure location too far forward of the base for these models. Better agreement is obtained between the potential theory and the experimental center of pressure location for the cylindrical afterbody models (figs. 4(b) and 4(d)) than for the boattail models (figs. 4(a) and 4(c)).

Inasmuch as the potential theory does not predict the rearward shift of the center of pressure with increasing angle of attack the discrepancy between the theoretical values and the data becomes more pronounced at the higher angles of attack.

The rearward shift of the center of pressure with angle of attack is predicted reasonably well for the boattail models by the method of reference 1. The calculated values are, however, too far forward of the base at all free-stream Mach numbers and angles of attack. For the cylindrical afterbody models the method of reference 1 predicted the center of pressure location accurately (figs. 4(b) and 4(d)). In general, the method of reference 1 shows a marked improvement in the prediction of the center of pressure location for the bodies of revolution, particularly for the boattailed bodies.

The variation of incremental fore drag coefficient with angle of attack for the four models at four Mach numbers is presented in figure 5. In general, the method of reference 1 predicts the increase of incremental fore drag with angle of attack, whereas the potential theory appreciably underestimates the measured values at the higher angle of attack. The underestimation of the incremental fore drag is associated with the inability of the potential theory to predict the normal force or the lift.

Comparison of the aerodynamic characteristics of models having the same ratio of base area to maximum area, but different fineness ratios are presented in figure 6 to show the effect of fineness ratio on the aerodynamic characteristics. These data show that increasing the fineness ratio from 12.2 to 14.2 resulted in an increase in the lift coefficient as might be expected from consideration of viscosity effects. The increase in lift coefficient at each angle of attack for both afterbody configurations was practically independent of the free-stream Mach number (figs. 6(a) and 6(b)).

Inasmuch as the increased fineness ratio for these models was obtained by inserting a cylindrical section of maximum diameter aft of station 45, it would be anticipated that a decrease of moment coefficient about station 45 would result from the increment of lift force.

This decrease of moment coefficient is evidenced in figures 6(c) and 6(d) which present the variation of the pitching-moment coefficient with free-stream Mach number for a range of angles of attack. The decrease in pitching-moment coefficient with increase in fineness ratio was larger for the cylindrical afterbody models than for the boattail models even though the lift coefficient increment was nearly the same for both configurations. This difference in decrease of moment coefficient may be attributed to an effectively larger moment arm for the resultant incremental normal force on the aft portion of the cylindrical afterbody model.

Although the lift increased and pitching moment about station 45 was reduced with increased fineness ratio, the center of pressure location as a percent of the model length was not changed appreciably as determined from figure 4.

The variation of the incremental fore drag coefficient with free-stream Mach number is presented in figures 6(e) and 6(f) for a range of angle of attack. These figures illustrate a slight increase in incremental fore drag coefficient with increase in fineness ratio at each angle of attack. The increase in this parameter with increased fineness ratio is virtually proportional to the increase in normal force coefficient inasmuch as the total axial force coefficient did not vary appreciably with this increase of fineness ratio.

The effect of boattailing on the aerodynamic characteristics is shown in figure 7. The higher lift coefficient obtained for the cylindrical afterbody models than for the boattail models at each angle of attack and free-stream Mach number can be attributed to the negative lift component over the boattail of models 1 and 3 (figs. 7(a) and 7(b)).

As might be anticipated, the negative lift component on the boattail models 1 and 3 resulted in an appreciable increase of pitching moment about station 45 as compared to the corresponding cylindrical afterbody model (figs. 7(c) and 7(d)). This increase in pitching moment is approximately independent of free-stream Mach number but increases with increasing angle of attack.

At each angle of attack a larger increase of moment coefficient between the cylindrical afterbody and boattail models was measured for the models having a fineness ratio of 14.2 than the models having a fineness ratio of 12.2. This larger increase in moment coefficient results from the difference in lift components between the boattail and cylindrical afterbody sections acting at a greater distance from the center of moments for the bodies of larger fineness ratio.

The variation of incremental fore drag with free-stream Mach number is presented in figures 7(e) and 7(f) for a range of angles of attack. The incremental fore drag was nearly independent of body shape at low angles of attack. For the bodies of fineness ratio 14.2 at  $10^\circ$  angle of attack, however, the higher incremental fore drag for the cylindrical afterbody model than the boattail model is largely due to the greater increase of the normal force of the cylindrical afterbody model compared to the boattail models.

Some indication of the effect of boattail convergence (defined as ratio of difference between maximum diameter and base diameter to twice the boattail length) on the aerodynamic characteristics can be obtained by comparing the results of model 1 with the data for the NACA RM-10 presented in reference 3. The two models were identical with respect to base area, maximum cross-sectional area, over-all length, and body shape for the first 7.5 maximum diameters of model length (that is, to station 45). The model of reference 3, however, had a boattail convergence ratio of approximately 0.074 as compared to a boattail convergence of 0.174 for model 1. The variation of lift, pitching moment, and incremental fore drag coefficients with free-stream Mach numbers for these two models is presented in figure 8 for a range of angles of attack. The lift coefficients presented in figure 8(a) are approximately equal and are not appreciably influenced by the change in boattail convergence of these two models. The pitching moment presented in figure 8(b), however, decreased for the larger boattail convergence, particularly at the higher free-stream Mach number and angles of attack. The lower pitching moment for model 1 compared to the model of reference 3 is not in agreement with the prediction based on linearized potential theory and is probably indicative of the influence of the body geometry on the viscosity effects. An appreciable increase in the incremental fore drag coefficient (fig. 8(c)) occurred with the decrease in boattail convergence at an angle of attack of  $6^\circ$  and  $8^\circ$ .

2127

The effect of afterbody shape on the drag parameters at  $0^\circ$  angle of attack can be determined from figure 9. The variation of total drag, boattail pressure drag, fore drag, and base drag coefficients with free-stream Mach number are presented for the models 1, 2, 3, and 4 and the model of references 2 and 3. These data were presumably influenced by tunnel flow irregularities (reference 3) at free-stream Mach numbers 1.50 and 1.60 but no corrections could be calculated for these effects because of the lack of pressure instrumentation. The data at free-stream Mach numbers of 1.79 and 1.99 were therefore extrapolated to 1.50 and 1.60 in accordance with the linear variations of the data observed in reference 3 to indicate the probable extent of the effect of the tunnel flow irregularities on the data.

The extrapolated curves indicate that the probable effect of the flow irregularities was to reduce the total drag coefficient at free-stream Mach numbers of 1.50 and 1.60 to a maximum of 6 percent (fig. 9(a)). The decrease in total-drag coefficient resulted primarily from the decrease in the base drag component (fig. 9(b)) and to a small extent by the reduction of the fore drag (fig. 9(c)) or more specifically the reduction of the boattail surface pressure drag (fig. 9(d)). (Boattail surface pressure drag for model 1 was computed as the difference in fore drags of models 1 and 2.)

Although the effect of fineness ratio (increased by adding a cylindrical section) on these drag components was small, the effect of boattailing was of significant proportion. The influence of boattailing on the drag components was determined by comparing the model having a cylindrical afterbody (model 2) with the models having the same forebody and fineness ratio (12.2) but with varying boattail convergence (0.174 and 0.074 on model 1 and the NACA RM-10, respectively).

The total drag of the model having a cylindrical afterbody was reduced approximately 30 percent by a boattail convergence of 0.174 (model 1) and decreased by approximately 45 percent by increasing the boattail length by decreasing the convergence to 0.074 (NACA RM-10). The reduction in total drag is effected primarily by the large reduction in the base drag of approximately 75 percent as a result of boattailing (fig. 9(b)); for the boattail models, the fore drag increased with increasing boattail convergence. The increased fore drag is due to the increased boattail surface pressure drag as shown in figure 9(d).

The variation of base pressure coefficient with free-stream Mach number for the configurations investigated and the model of reference 3 is presented in figure 10 at an angle of attack of  $0^\circ$ . The effect of boattailing was to decrease the magnitude of the negative base pressure coefficient compared to the base pressure coefficient of the cylindrical afterbody models.

A hysteresis effect on base pressure with increasing and decreasing angle of attack as reported in reference 3 was also noted in this investigation. The average values, however, were presented as the increment of base pressure coefficient with angle of attack at four Mach numbers in figures 11(a) to 11(d). The effects of fineness ratio and boattailing on these data are not distinct. However, a qualitative estimate of the effect of angle of attack on the base pressure coefficient can be determined from figure 11.

2127

#### SUMMARY OF RESULTS

The aerodynamic characteristics of four slender pointed-nose bodies of revolution were investigated in the NACA Lewis 8- by 6-foot supersonic wind tunnel at a Reynolds number of approximately  $35 \times 10^6$  and at free-stream Mach numbers of 1.50, 1.60, 1.79, and 1.99 through a range of angles of attack. From this investigation the following results were obtained:

1. Increasing the model fineness ratio from 12.2 to 14.2 by adding a cylindrical section did not appreciably affect the measured total drag, base drag, fore drag, or the base pressure coefficient at zero angle of attack. The increase in model fineness ratio resulted in an increase in the incremental fore drag and lift coefficient at angle of attack. The center of pressure location as a percent of the body length was not changed by the increase in body fineness ratio.
2. At an angle of attack of  $0^\circ$ , boattailing increased the model fore drag but decreased the measured base drag appreciably with a resultant decrease of total drag. The measured base pressure coefficient was also decreased. At angle of attack, boattailing produced an increase in pitching moment about the station of maximum diameter located approximately 7.5 maximum diameters from the nose and a decrease in lift and incremental fore drag.
3. Decreasing the boattail convergence from approximately 0.174 to 0.074 increased the measured base drag but reduced the model fore drag with a resultant decrease of the model total drag at  $0^\circ$  angle of attack. With increasing angle of attack, the lift was not appreciably affected by the change in boattail convergence but the pitching moment about station 45 and the incremental fore drag were increased.
4. The method developed by Allen (reference 1) was a significant improvement over the linearized potential theory in predicting the aerodynamic characteristics of bodies of revolution investigated, particularly at the higher angles of attack.

2127

5. For the cylindrical afterbody models, use of Allen's method overestimated the lift coefficient above  $2^\circ$  angle of attack at all free-stream Mach numbers but predicted the center of pressure location quite accurately for these conditons. For the boattail models at all angles of attack, the Allen method generally was in good agreement with the lift coefficients at the low free-stream Mach numbers but predicted the center of pressure location too far forward of the base at all free-stream Mach numbers.

Lewis Flight Propulsion Laboratory,  
National Advisory Committee for Aeronautics,  
Cleveland, Ohio, September 15, 1950.

#### REFERENCES

1. Allen, H. Julian: Estimation of the Forces and Moments Acting on Inclined Bodies of Revolution of High Fineness Ratio. NACA RM A9I26, 1949.
2. Luidens, Roger W., and Simon, Paul C.: Aerodynamic Characteristics of NACA RM-10 Missile in 8- by 6-Foot Supersonic Wind Tunnel at Mach numbers from 1.49 to 1.98. I - Presentation and Analysis of Pressure Measurements (Stabilizing Fins Removed). NACA RM E50D10, 1950.
3. Esenwein, Fred T., Obery, Leonard J., and Schueller, Carl F.: Aerodynamic Characteristics of NACA RM-10 Missile in 8- by 6-Foot Supersonic Wind Tunnel at Mach Numbers from 1.49 to 1.98. II - Presentation and Analysis of Force Measurements. NACA RM E50D28, 1950.
4. Tsien, Hsue-Shen: Supersonic Flow over an Inclined Body of Revolution. Jour. Aero. Sci., vol. 5, no. 12, Oct. 1938, pp. 480-483.
5. Chapman, Dean R.: An Analysis of Base Pressure of Supersonic Velocities and Comparison with Experiment. NACA TN 2137, 1950.
6. Perkins, Edward W.: Experimental Investigation of the Effects of Support Interference on the Drag of Bodies of Revolution at a Mach Number of 1.5. NACA RM ASB05, 1948.
7. Luidens, Roger W., and Simon, Paul C.: Aerodynamic Characteristics of NACA RM-10 Missile in 8- by 6-Foot Supersonic Wind Tunnel at Mach Numbers from 1.49 to 1.98. III - Analysis of Force Distribution at Angle of Attack (Stabilizing Fins Removed). NACA RM E50I19, 1950.

TABLE I - EQUATIONS FOR MODEL CONTOURS

Model	$r = x\sqrt{c/2} (2-x/45)$	$r = 3$	$r = (x_1^2/a) + 3; x_1 = (x-x_0)$
1	0 ≤ x ≤ 45	45 ≤ x ≤ 61.25	61.25 ≤ x ≤ 73.25; x <sub>0</sub> = 61.25
2	0 ≤ x ≤ 45	45 ≤ x ≤ 73.25	-----
3	0 ≤ x ≤ 45	45 ≤ x ≤ 73.00	73.00 ≤ x ≤ 85.00; x <sub>0</sub> = 73.00
4	0 ≤ x ≤ 45	45 ≤ x ≤ 85.00	-----

r = radius    x = model station    c = 2/(15)<sup>2</sup>    a = - 121.8

Ordinates of models 1, 2, 3, 4, to station 61.25

Station	Radius	Station	Radius	Station	Radius
0	0	20	2.074	40	2.963
2	.260	22	2.216	42	2.986
4	.509	24	2.348	44	2.998
6	.746	26	2.465	45	3.000
8	.970	28	2.573	45	3.000
10	1.185	30	2.667	45	3.000
12	1.386	32	2.749	45	3.000
14	1.576	34	2.820	45	3.000
16	1.754	36	2.880	45	3.000
18	1.950	38	2.927	61.25	3.000

Station	Model			
	1	2	3	4
	Radius	Radius	Radius	Radius
61.25	3.000	3.000	3.000	3.000
62	2.995	3.000	3.000	3.000
64	2.986	3.000	3.000	3.000
66	2.823	3.000	3.000	3.000
68	2.727	3.000	3.000	3.000
70	2.576	3.000	3.000	3.000
72	2.055	3.000	3.000	3.000
73	1.867	3.000	3.000	3.000
73.25	1.818	3.000	3.000	3.000
74			2.992	3.000
76			2.926	3.000
78			2.795	3.000
80			2.598	3.000
82			2.535	3.000
84			2.005	3.000
85			1.818	3.000



TABLE II - TEST REYNOLDS NUMBER BASED ON MODEL LENGTH

Free-stream Mach number M <sub>0</sub>	Model			
	1	2	3	4
1.50	28,800,000	29,200,000	31,200,000	34,200,000
1.60	30,700,000	30,100,000	32,100,000	35,900,000
1.79	32,700,000	31,700,000	35,200,000	38,200,000
1.99	32,600,000	33,400,000	36,000,000	39,500,000

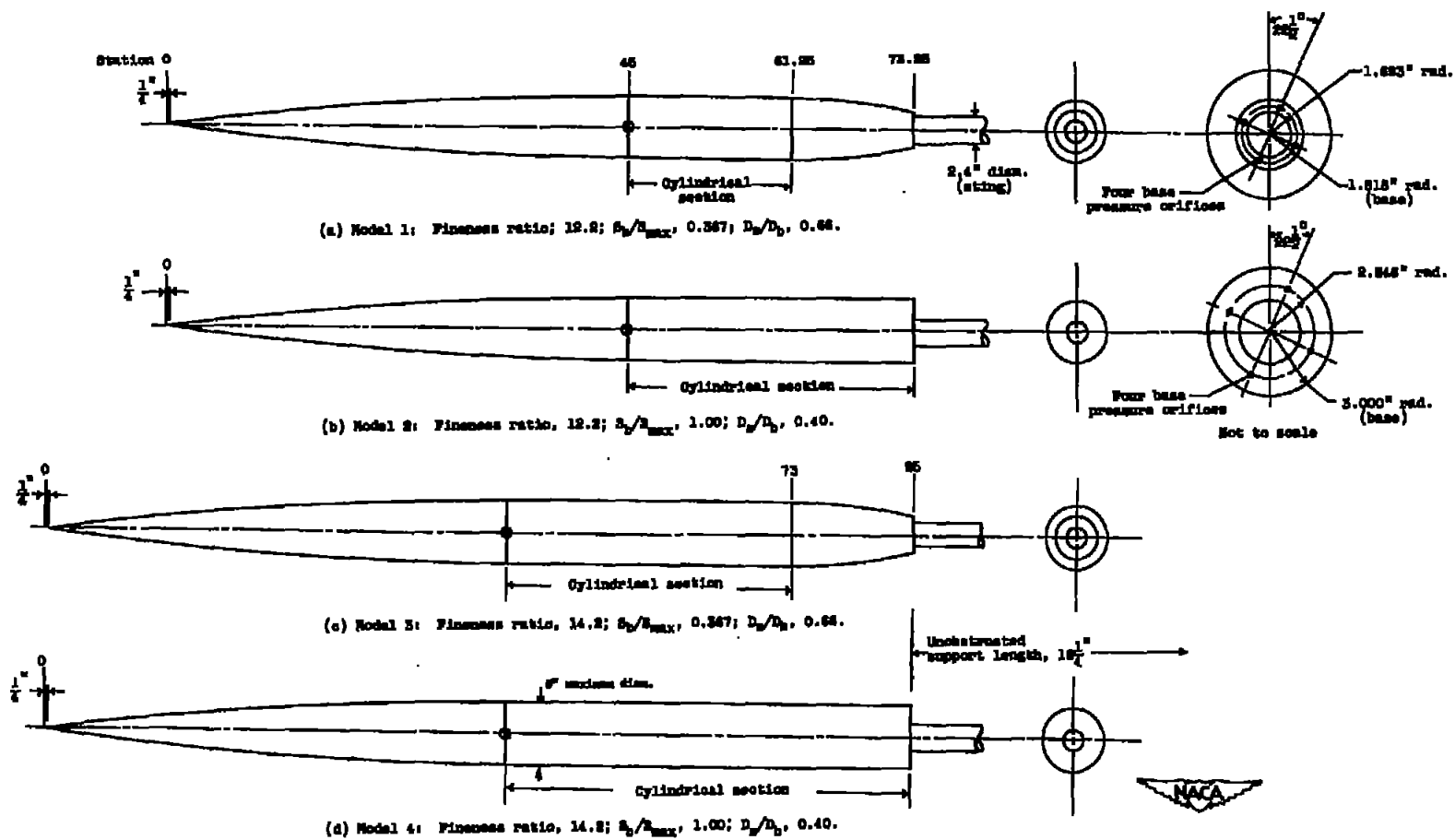


Figure 1. - Schematic diagram of four configurations investigated showing principal details and base pressure orifice location.

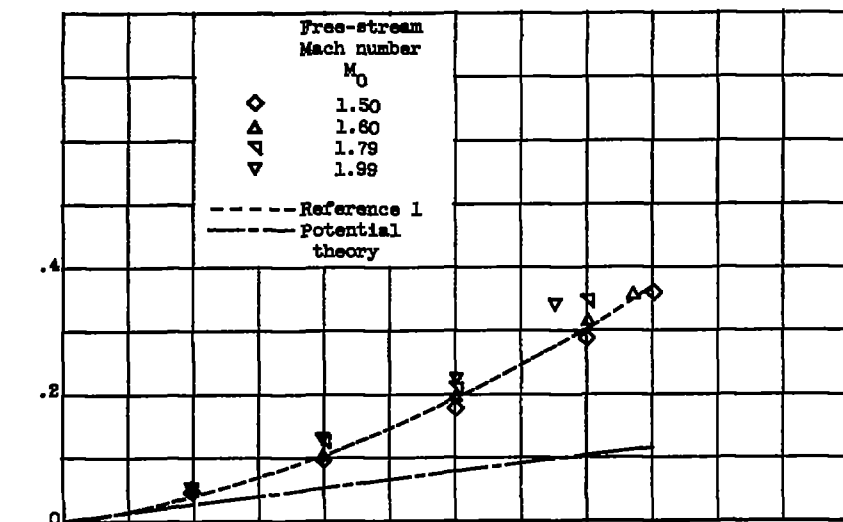
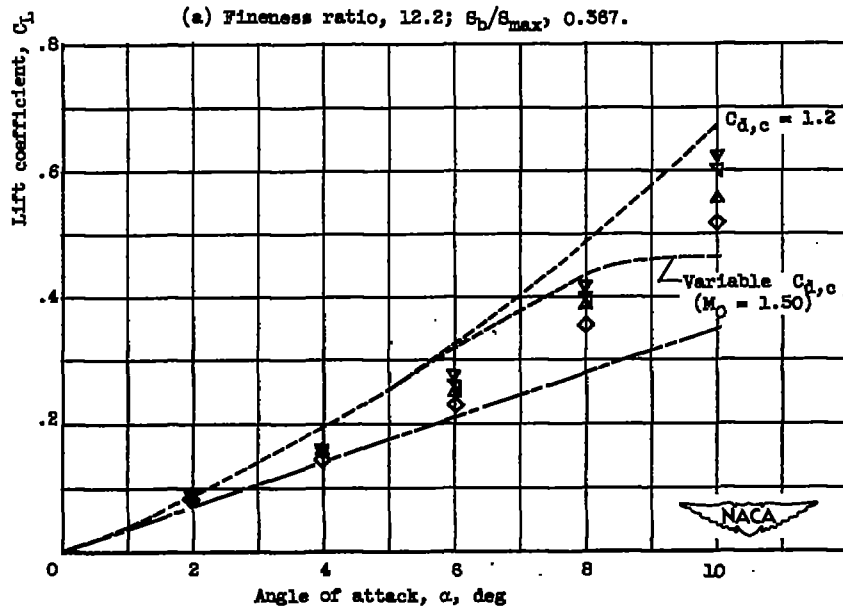
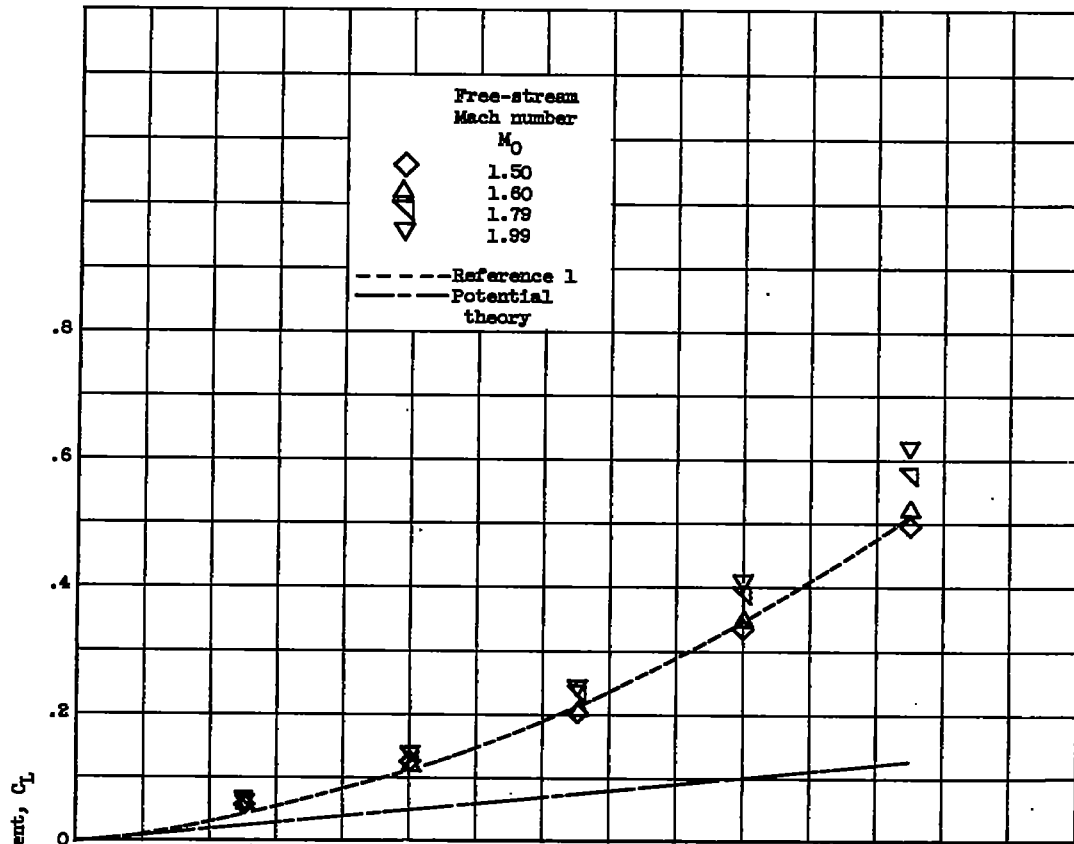
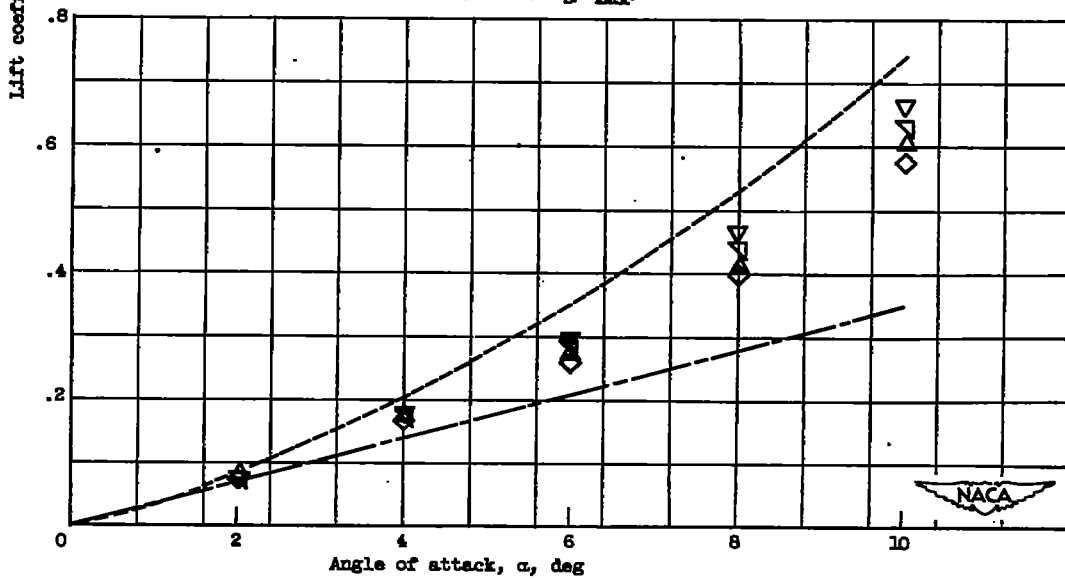
(a) Fineness ratio, 12.2;  $S_0/S_{max}$ , 0.567.(b) Fineness ratio, 12.2;  $S_0/S_{max}$ , 1.00.

Figure 2. - Variation of lift coefficient with angle of attack at four Mach numbers for four models investigated.

2127



(c) Fineness ratio, 14.2;  $S_b/S_{max}$ , 0.387.



(d) Fineness ratio, 14.2;  $S_b/S_{max}$ , 1.00.

Figure 2. - Concluded. Variation of lift coefficient with angle of attack at four Mach numbers for four models investigated.

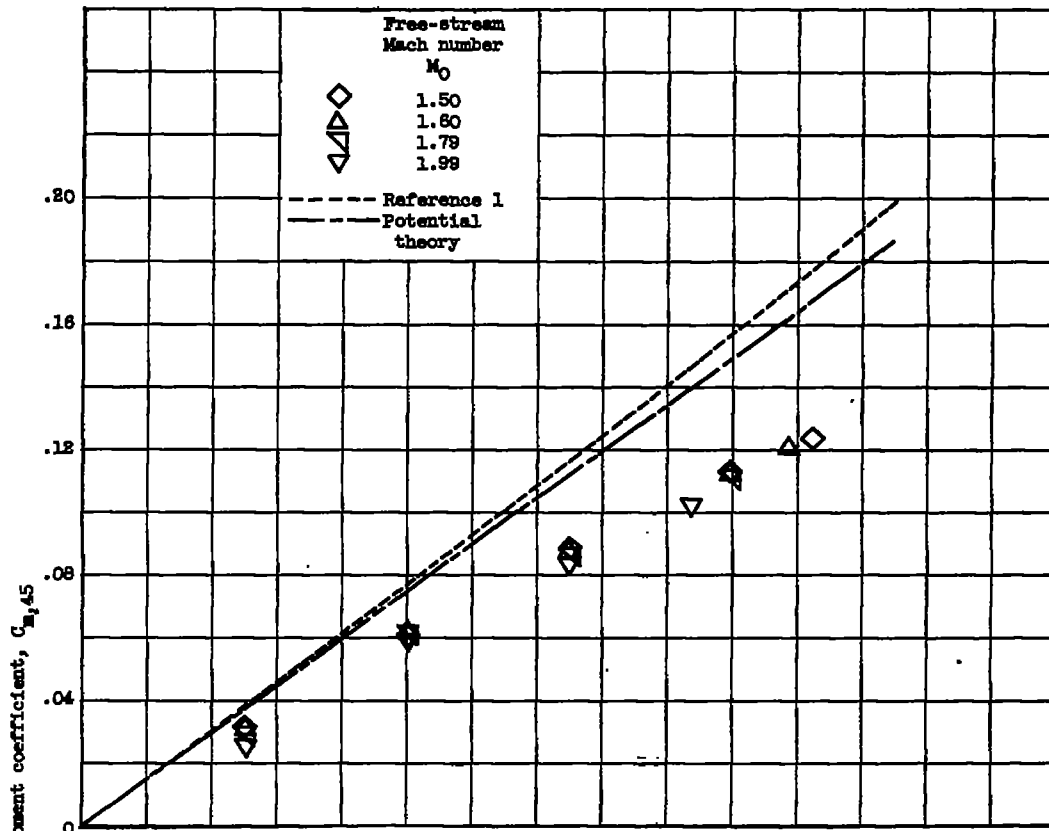
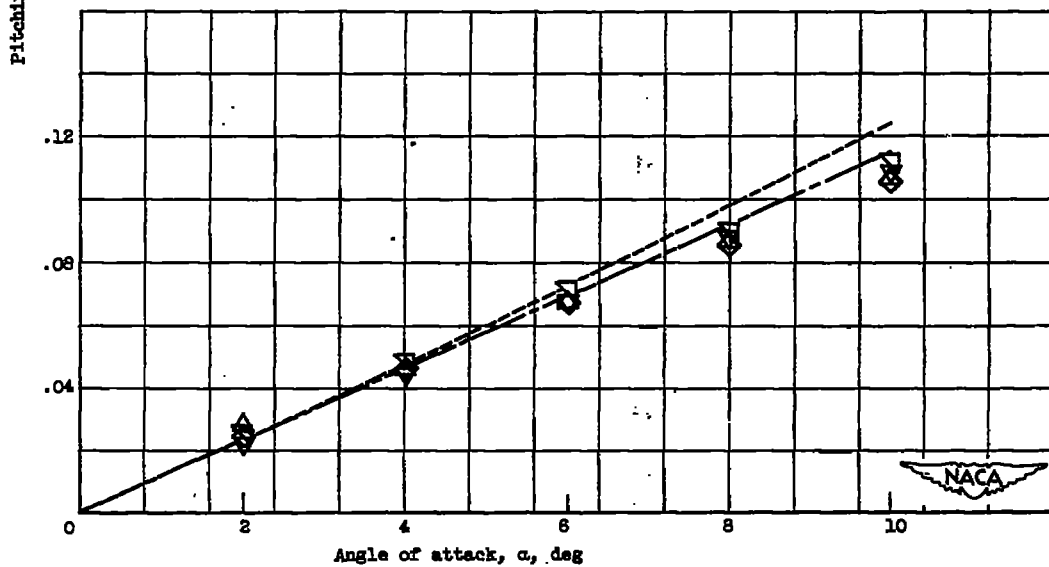
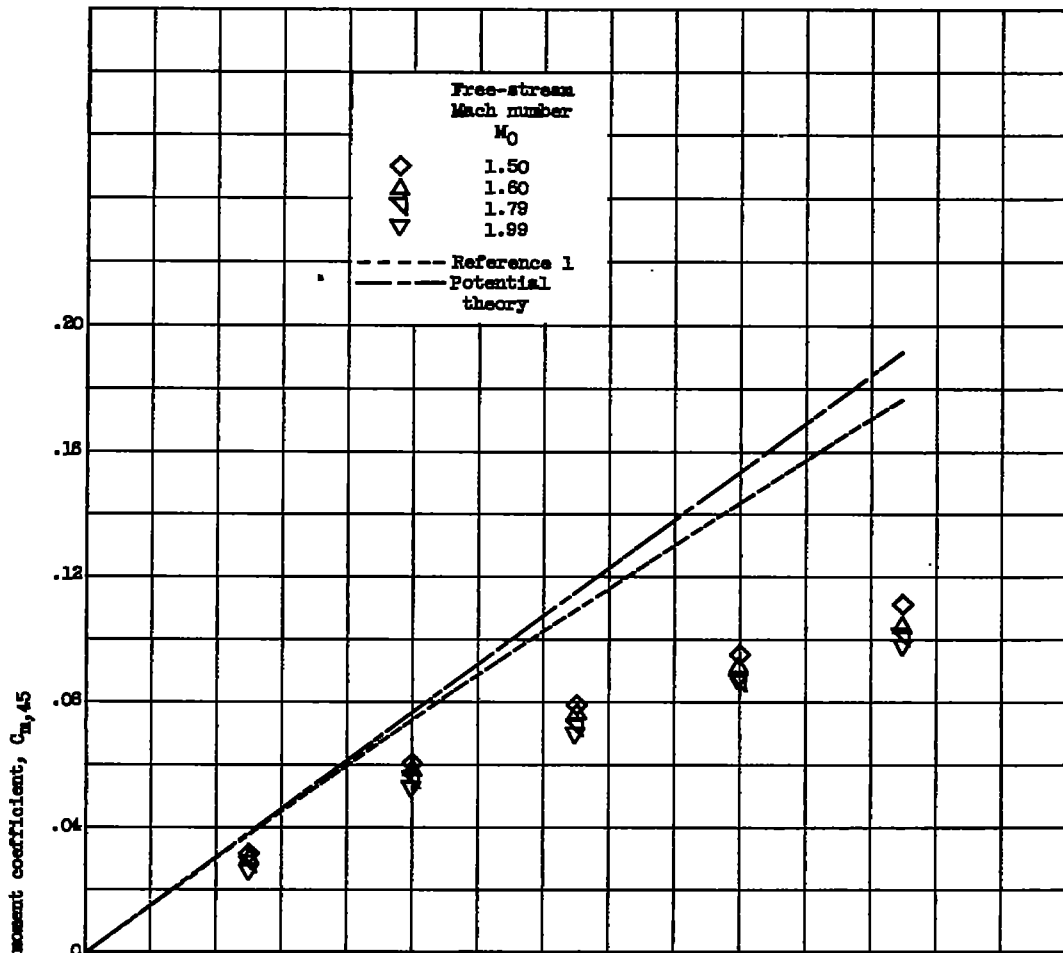
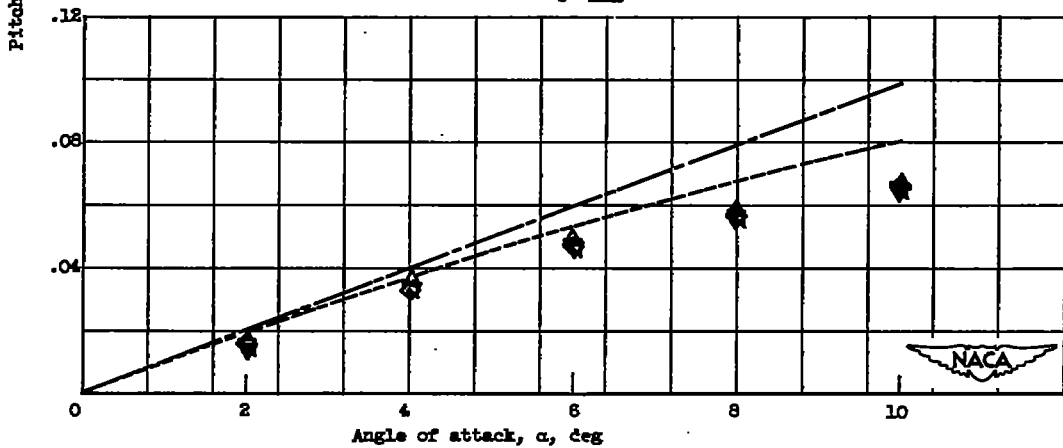
(a) Fineness ratio, 12.2;  $S_b/S_{max}$ , 0.567.(b) Fineness ratio, 12.2;  $S_b/S_{max}$ , 1.00.

Figure 3. - Variation of pitching-moment coefficient with angle of attack at four Mach numbers for four models investigated.

2127



(c) Fineness ratio, 14.2;  $S_b/S_{max}$ , 0.567.



(d) Fineness ratio, 14.2;  $S_b/S_{max}$ , 1.00.

Figure 3. - Concluded. Variation of pitching-moment coefficient with angle of attack at four Mach numbers for four models investigated.

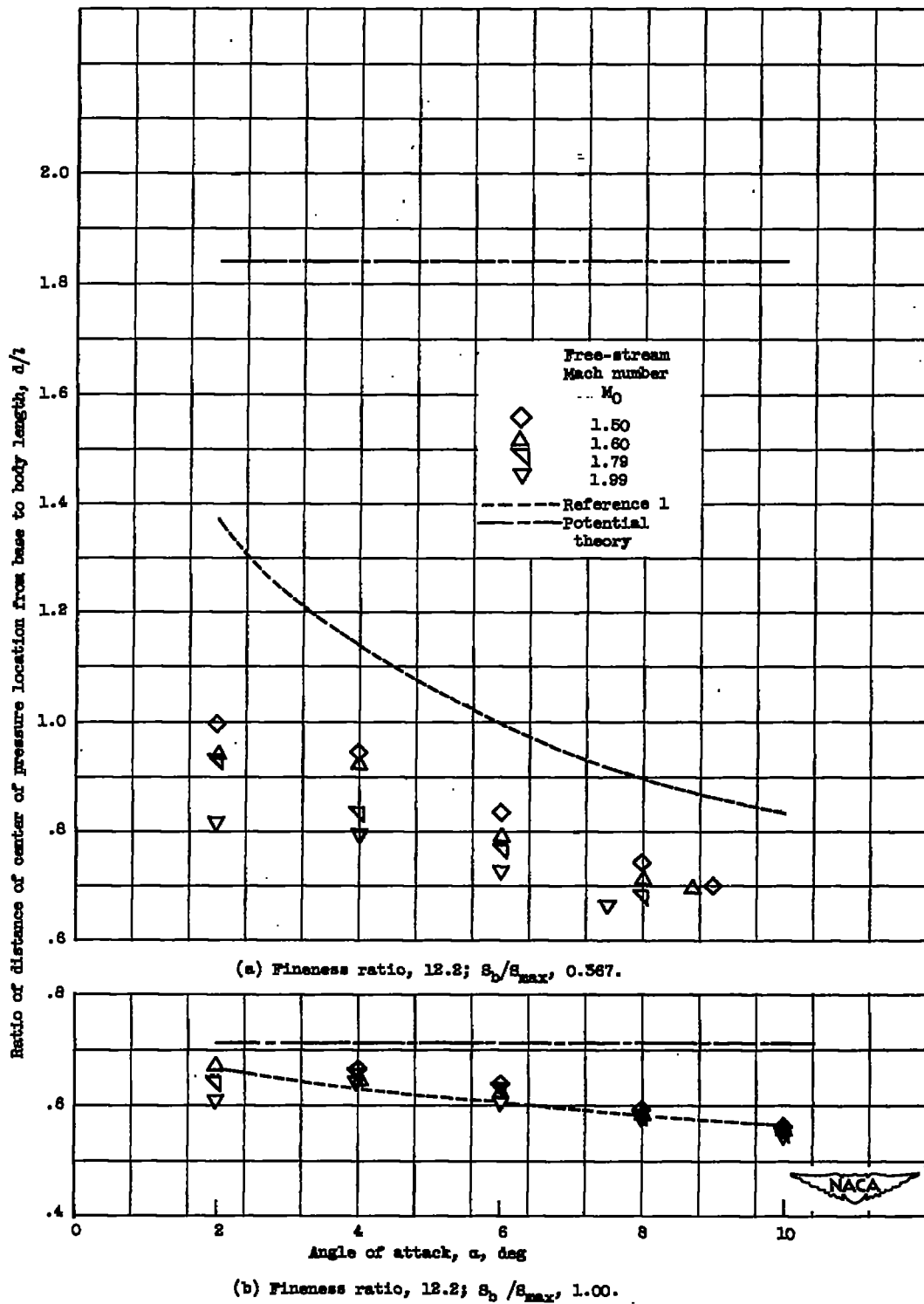
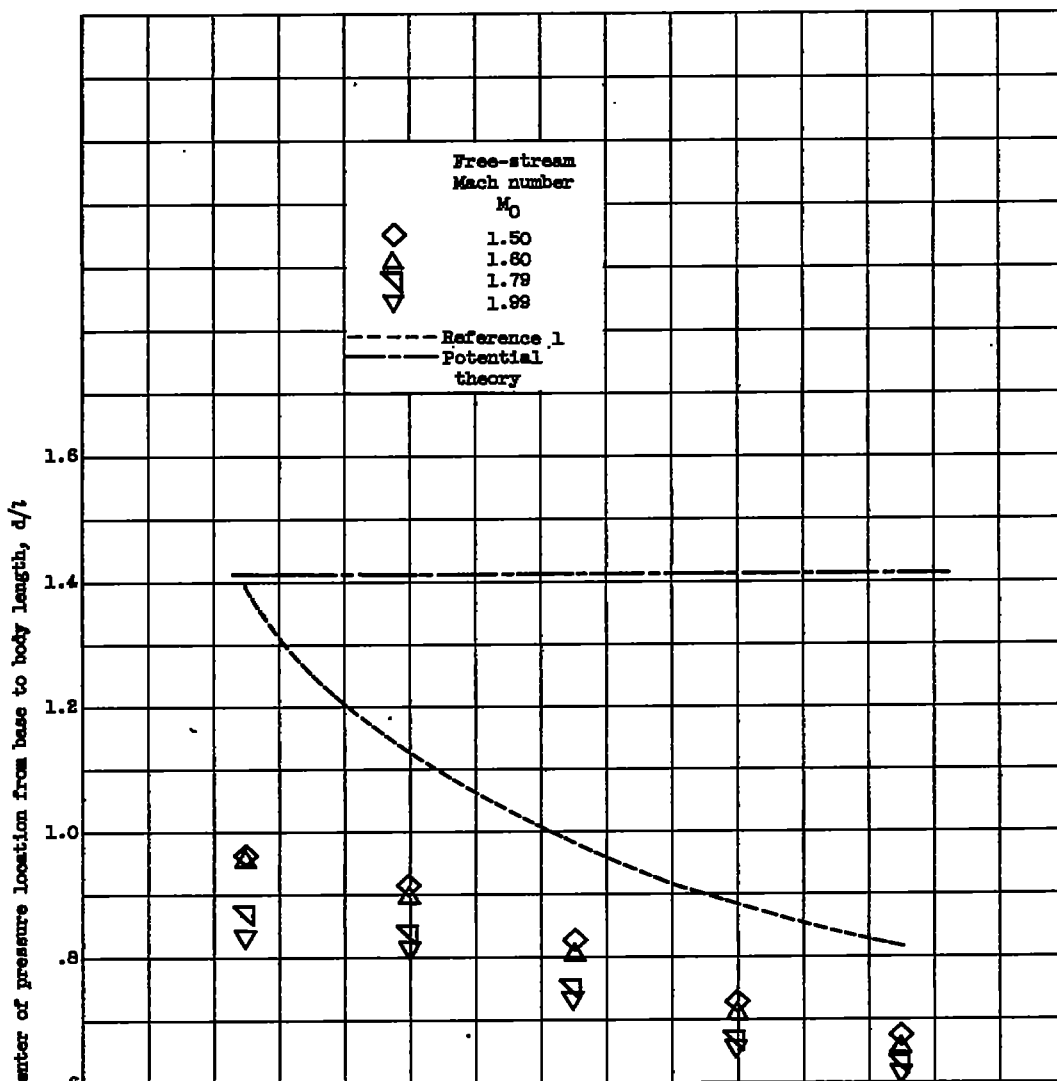
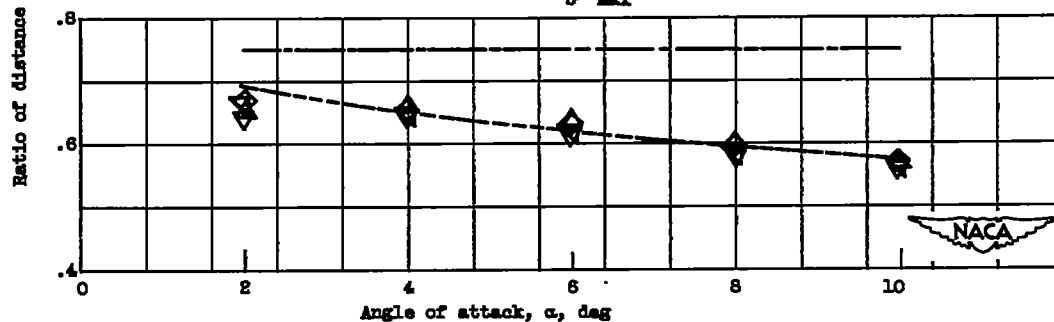


Figure 4. - Variation of ratio of distance of center of pressure location from base to body length with angle of attack at four Mach numbers for four models investigated

2127



(c) Fineness ratio, 14.2;  $S_b/S_{max}$ , 0.367.



(d) Fineness ratio, 14.2;  $S_b/S_{max}$ , 1.00.

Figure 4. - Concluded. Variation of ratio of distance of center of pressure location from base to body length with angle of attack at four Mach numbers for four models investigated.

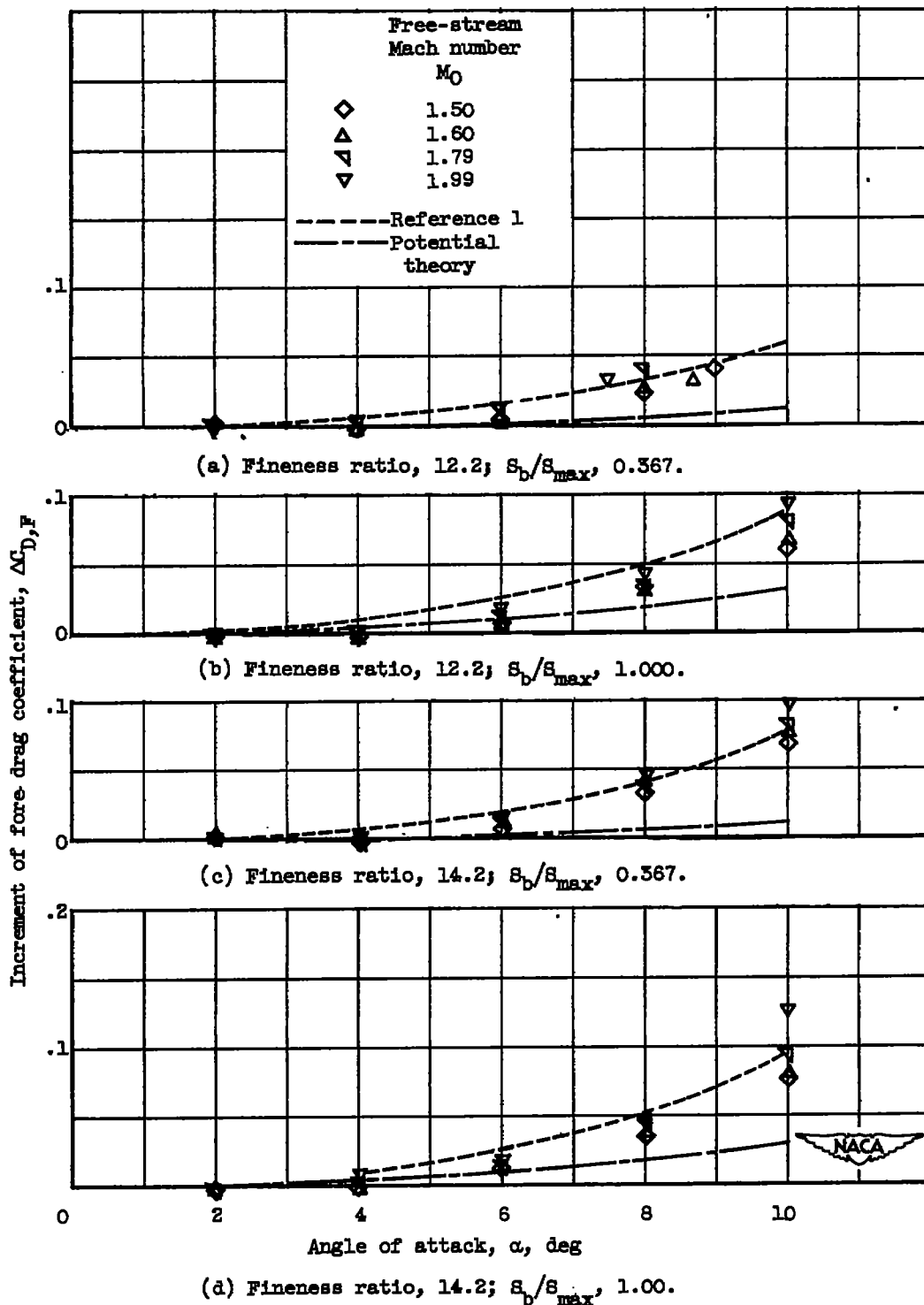


Figure 5. - Variation of increment of fore drag coefficient with angle of attack at four Mach numbers for four models investigated.

2127

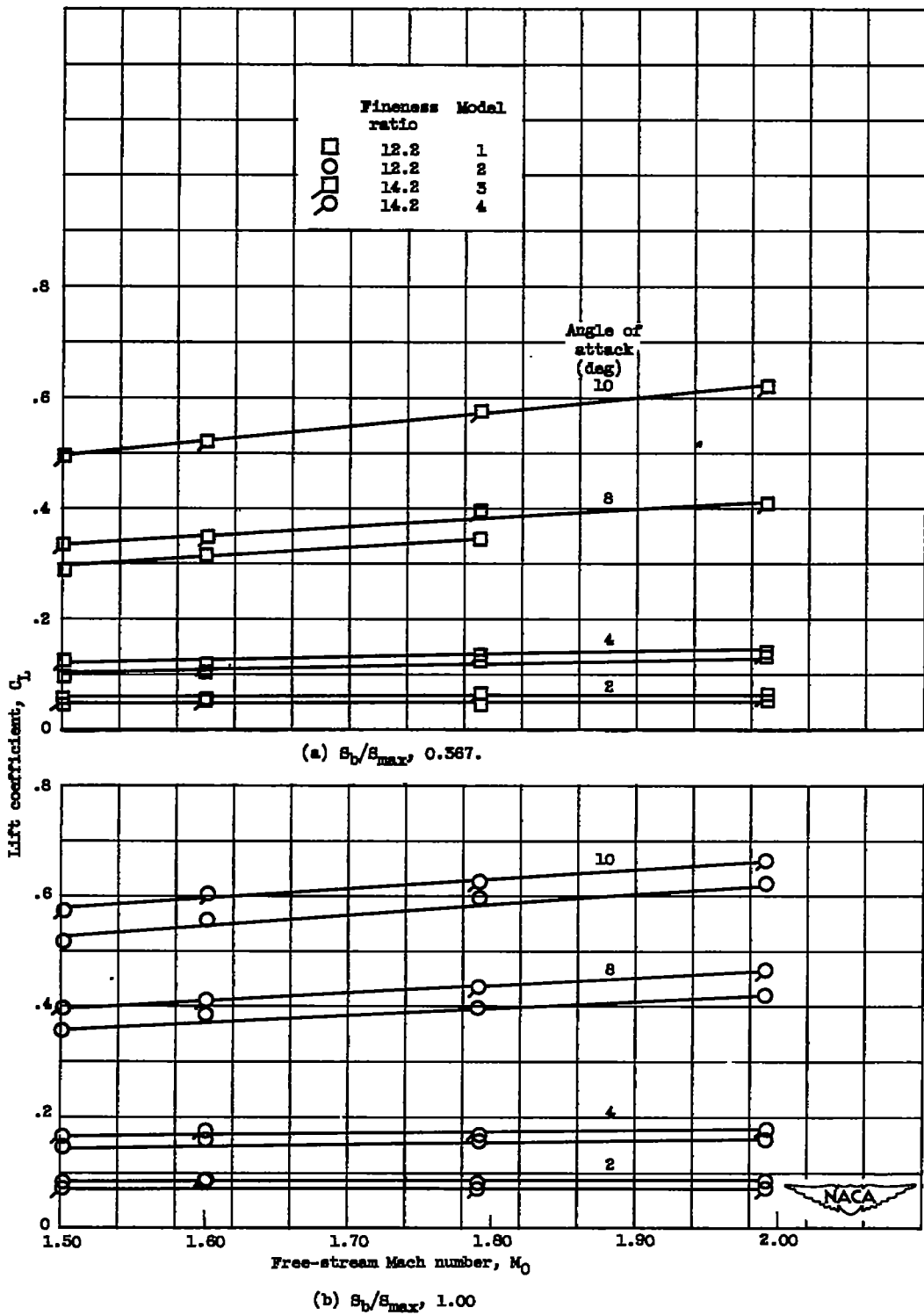


Figure 8. - Effect of fineness ratio on aerodynamic characteristics of four models investigated.

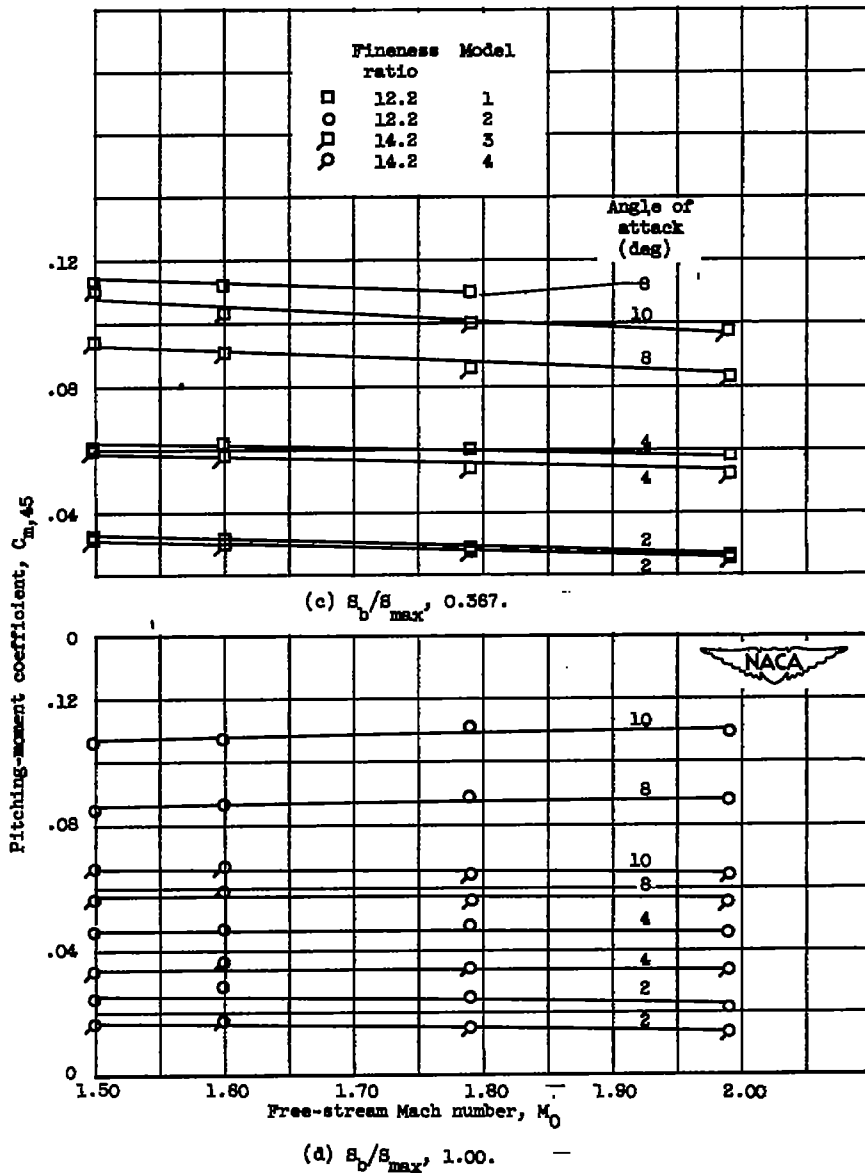


Figure 6. - Continued. Effect of fineness ratio on aerodynamic characteristics of four models investigated.

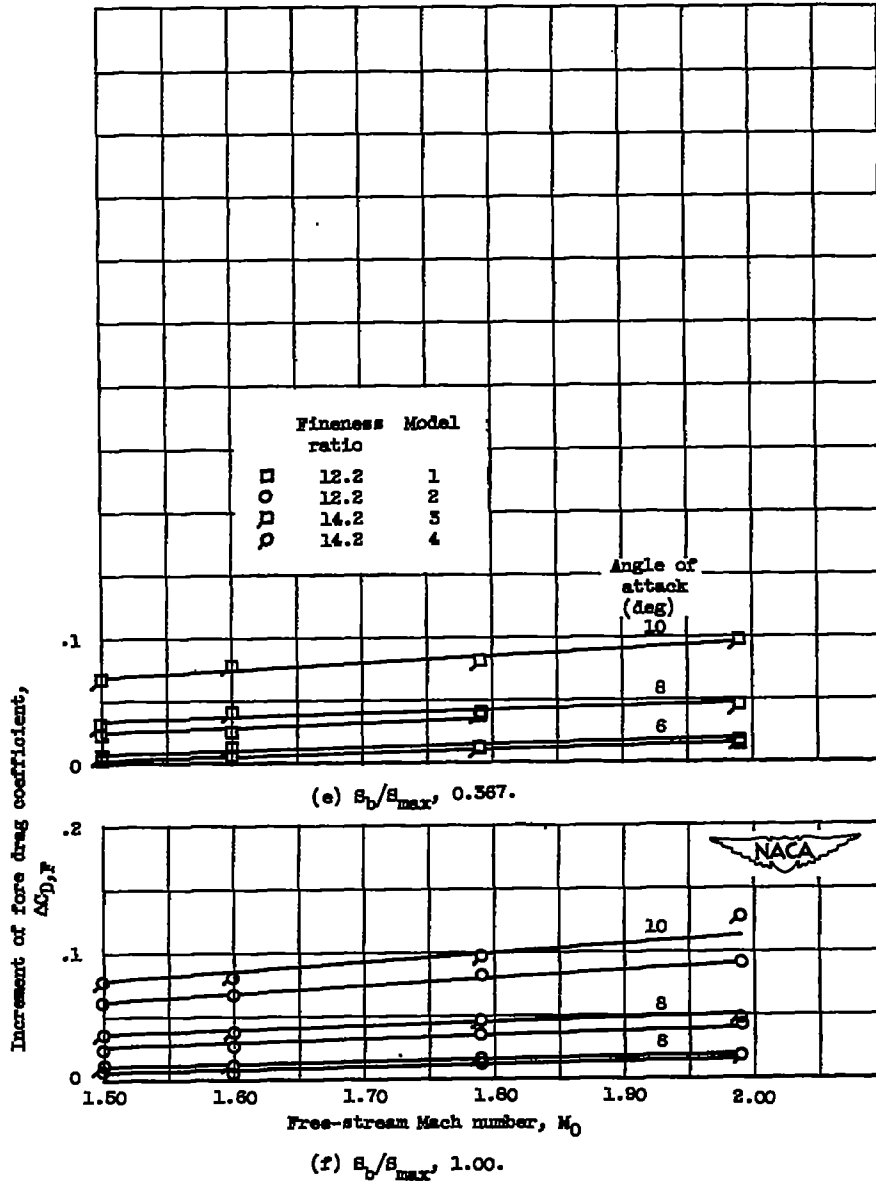
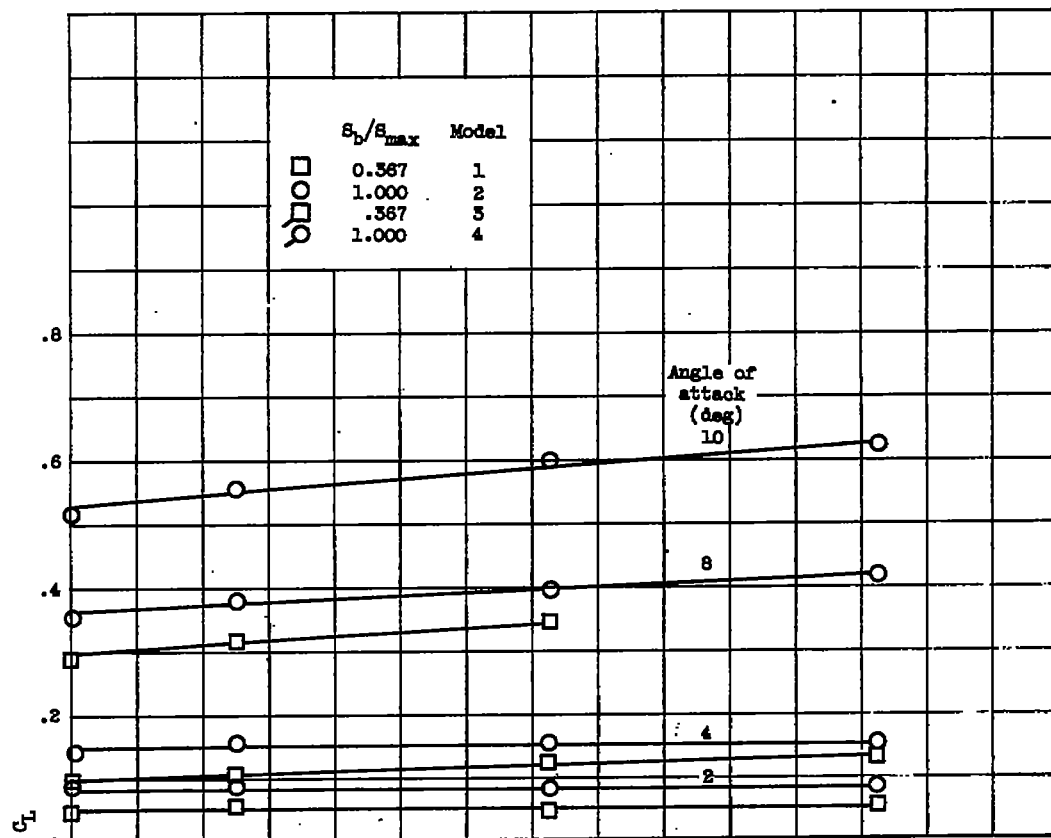
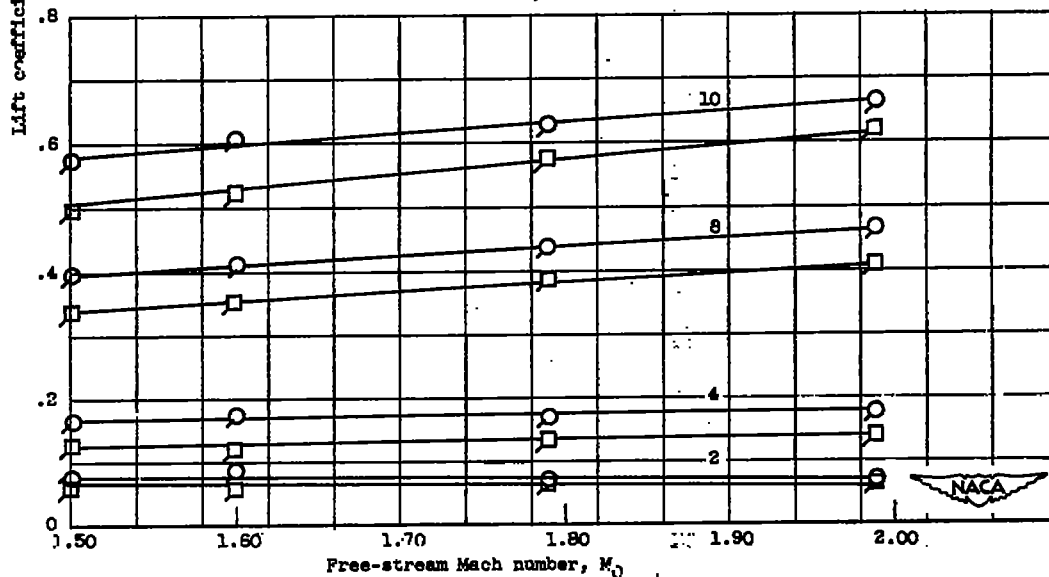


Figure 8. - Concluded. Effect of fineness ratio on aerodynamic characteristics of four models investigated.

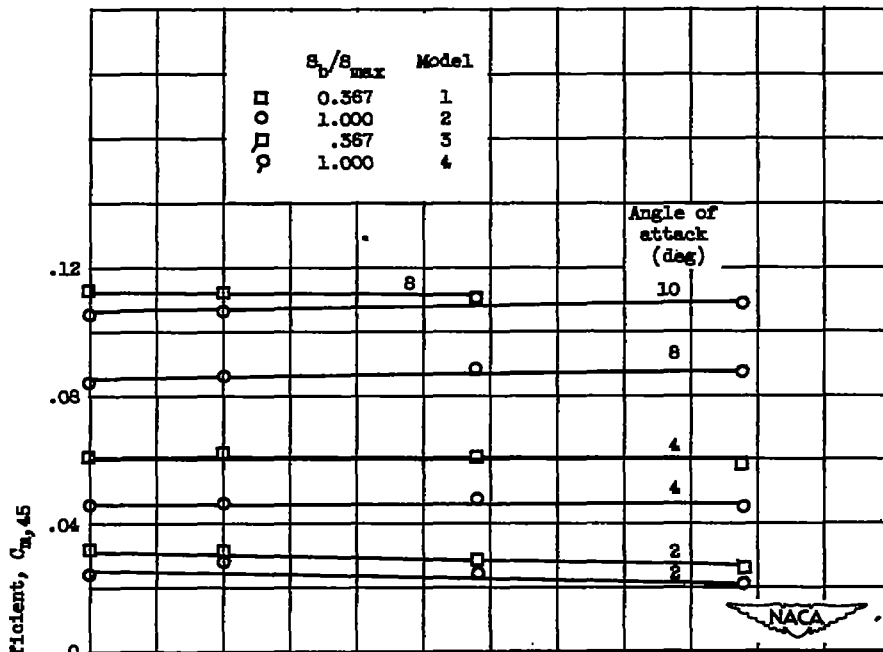


(a) Fineness ratio, 12.2

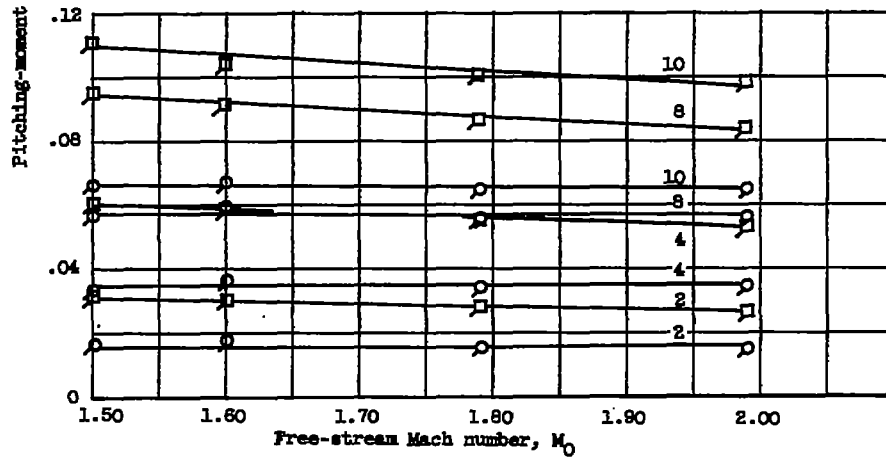


(b) Fineness ratio, 14.2.

Figure 7. - Effect of boattailing on aerodynamic characteristics of four models investigated.



(c) Fineness ratio, 12.2.



(d) Fineness ratio, 14.2.

Figure 7. - Continued. Effect of boattailing on aerodynamic characteristics of four models investigated.

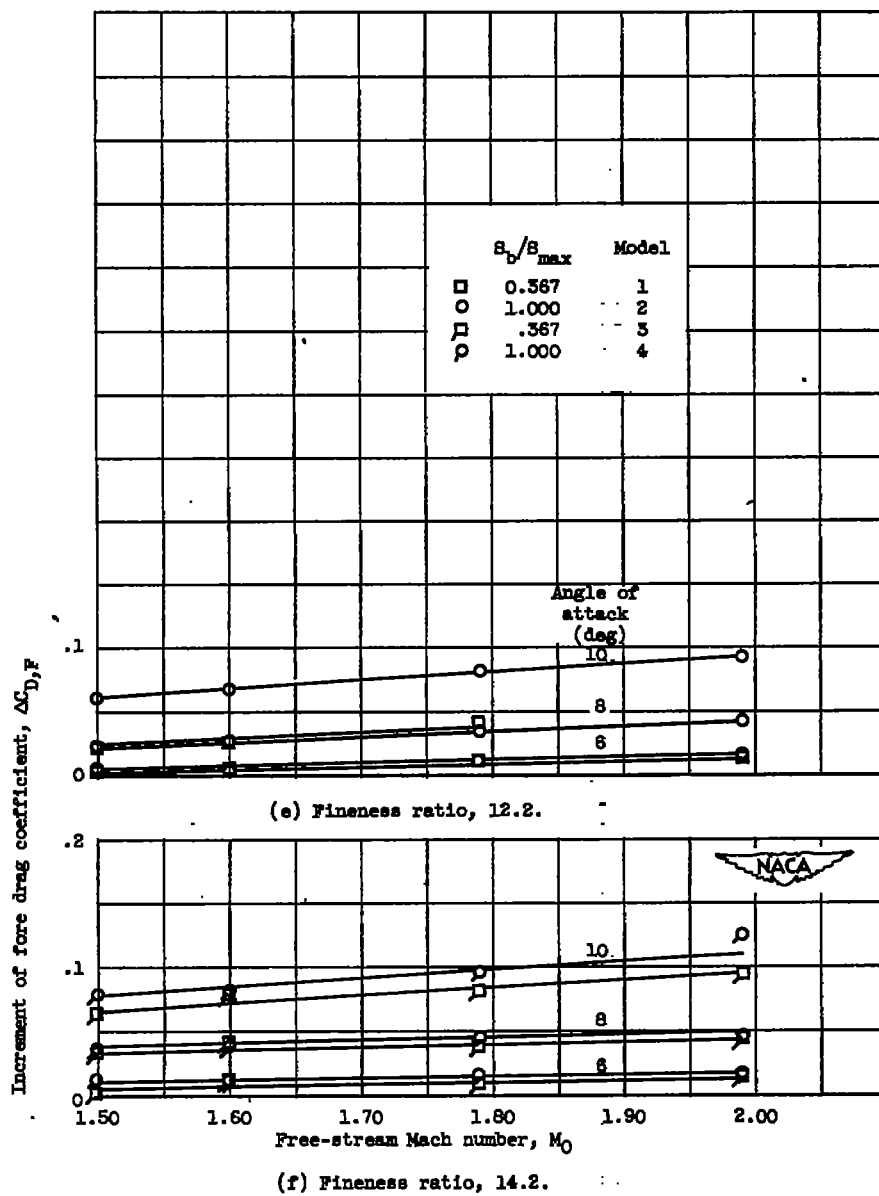
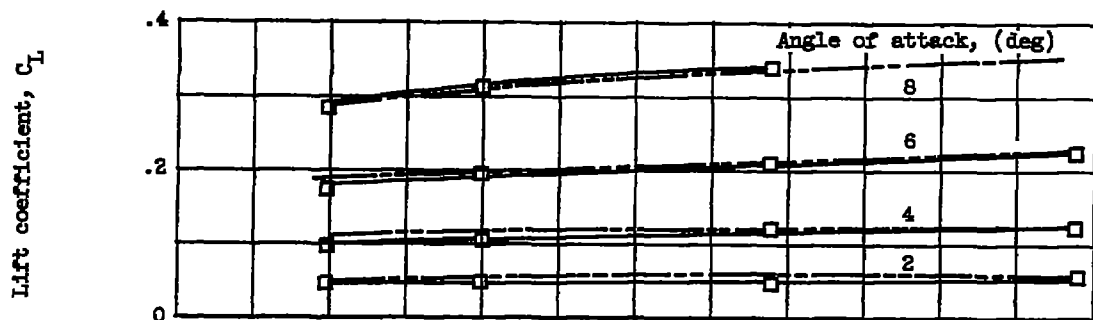
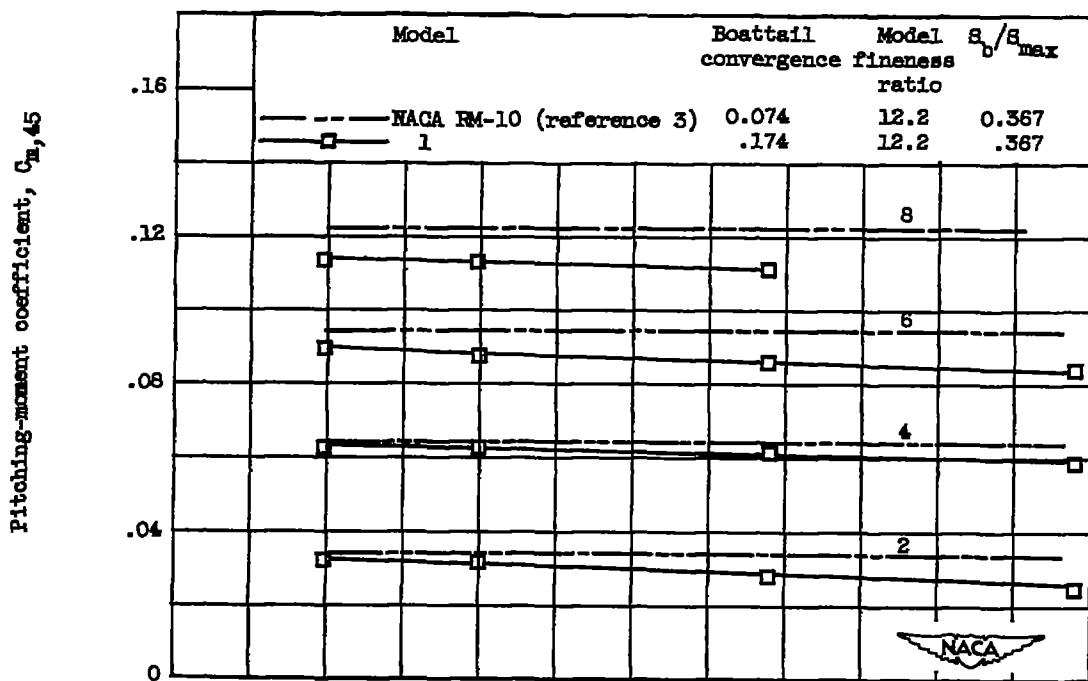


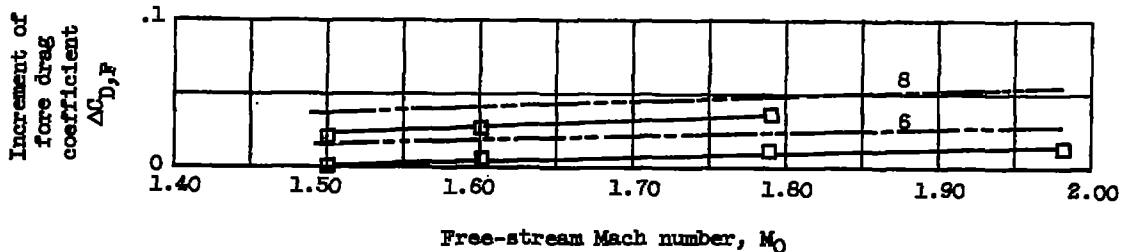
Figure 7. - Concluded. Effect of boattailing on aerodynamic characteristics of four models investigated.



(a) Lift coefficient.



(b) Pitching-moment coefficient.



(c) Increment of fore drag coefficient.

Figure 8. - Effect of boattail convergence on aerodynamic characteristics.

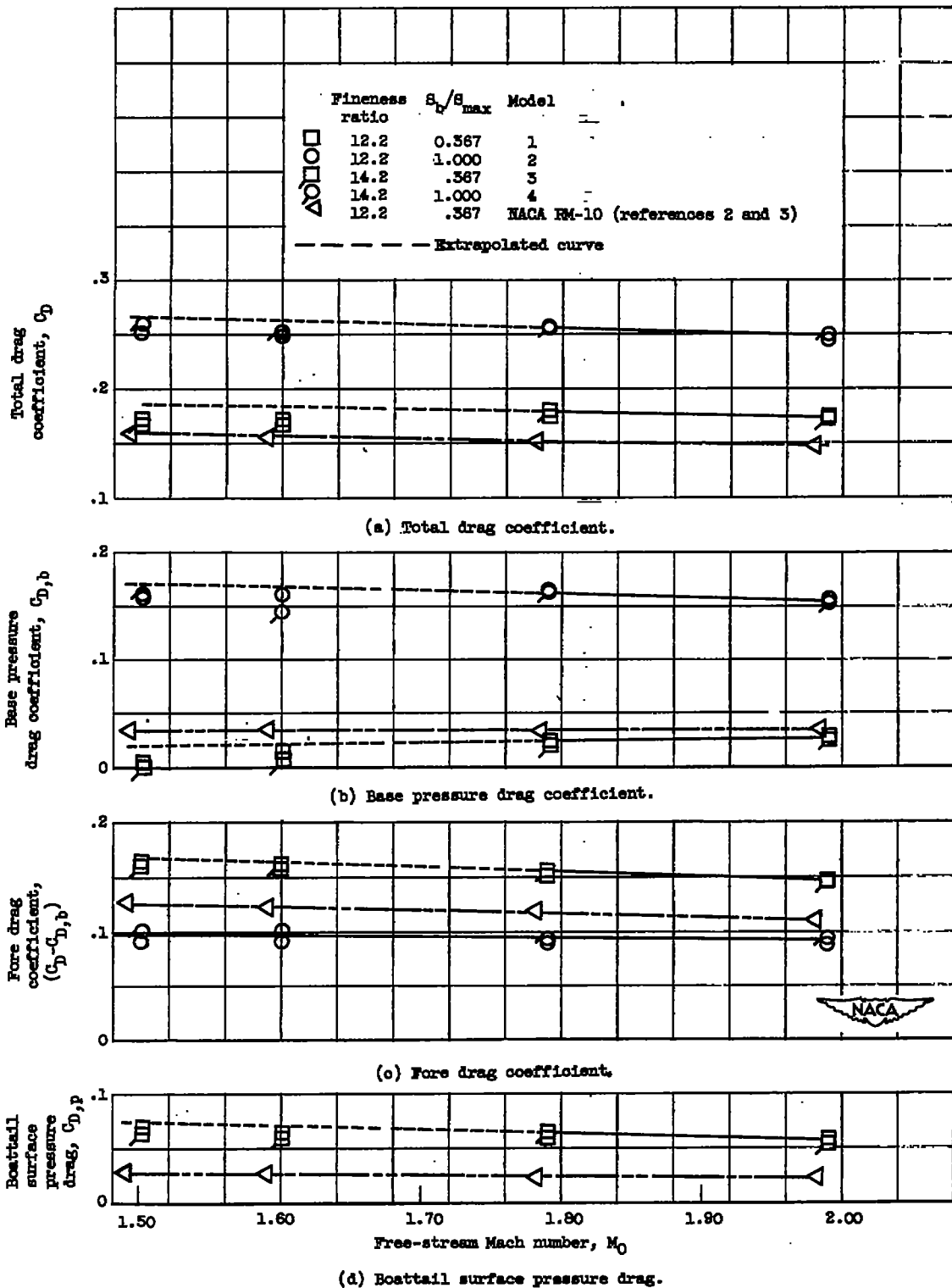


Figure 9. - Effect of fineness ratio and afterbody shape on drag coefficients at angle of attack of  $0^\circ$ .

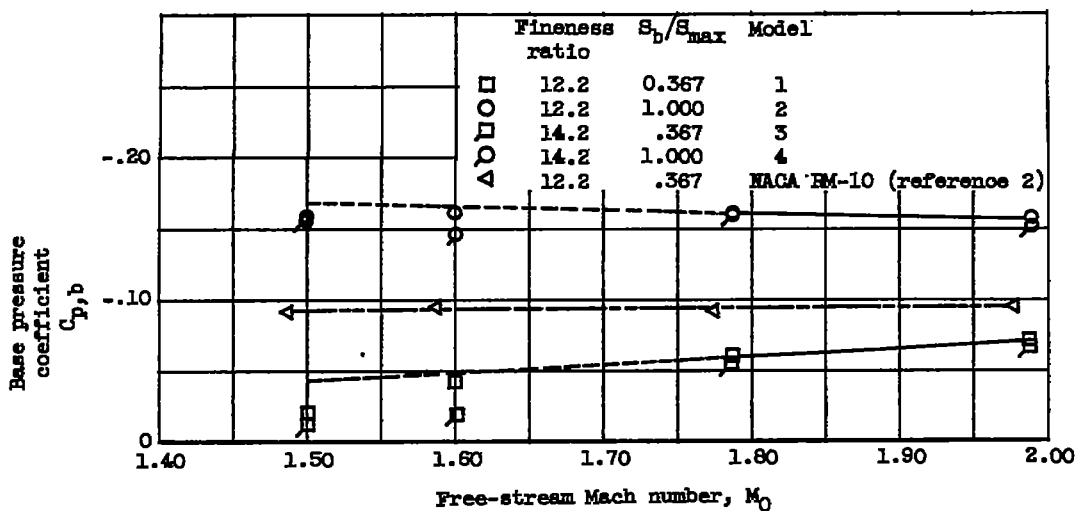


Figure 10. - Variation of base pressure coefficient with Mach number at angle of attack of 0°.

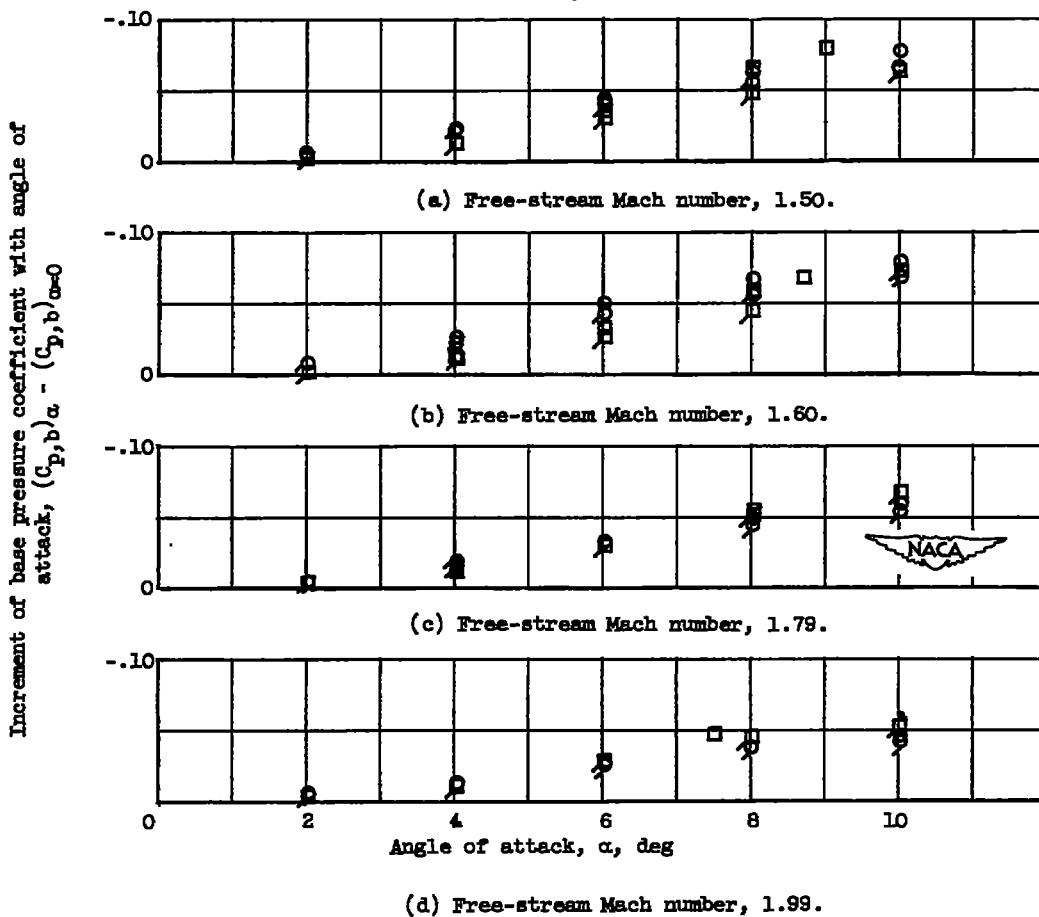


Figure 11. - Variation of increment of base pressure coefficient with angle of attack of various Mach numbers for four models investigated.